



Contents lists available at ScienceDirect

# Thermal Science and Engineering Progress

journal homepage: [www.sciencedirect.com/journal/thermal-science-and-engineering-progress](http://www.sciencedirect.com/journal/thermal-science-and-engineering-progress)

## Numerical analysis of non-Darcian mixed convection flows in a ventilated enclosure filled with a fluid-saturated porous medium

Wissam H. Alawee<sup>a</sup>, Gazy F. Al-Sumaily<sup>a,b,\*</sup>, Hayder A. Dhahad<sup>c</sup>, Mark C. Thompson<sup>b</sup><sup>a</sup> Workshop and Training Centre, University of Technology, Baghdad, Iraq<sup>b</sup> Department of Mechanical and Aerospace Engineering, Monash University, Victoria 3800, Australia<sup>c</sup> Mechanical Engineering Department, University of Technology, Baghdad, Iraq

### ARTICLE INFO

#### Keywords:

Mixed convection  
 Vented enclosure  
 Laminar aiding flow  
 Porous media

### ABSTRACT

Transient combined forced and natural convection in a square enclosure vertically ventilated and stuffed with an air-saturated fibrous material is studied numerically. This investigation employs the full Brinkman-Forchheimer-extended Darcy model for estimating the fluid flow, coupled with the one-equation energy model for estimating the temperature distribution and heat transfer. The pertinent parameters are Richardson number ( $Ri = 0-30$ ), Reynolds number ( $Re = 50-300$ ), Darcy number ( $Da = 0.01-100$ ), the solid/fluid thermal conductivity ratio ( $K_r = 1-10^5$ ), the porosity ( $\epsilon = 0.5-0.95$ ), and the inlet/outlet openings width ( $d/H = 0.05-0.3$ ). The obtained results show that the existence of the porous material augments considerably the mean Nusselt number  $Nu_m$  in general, and further increase in  $Nu_m$  can be acquired as Reynolds and/or Richardson numbers increases. Also, increasing the inlet/outlet ports width increases  $Nu_m$ , with an optimum value at  $d/H = 0.25$  for acquiring maximum  $Nu_m$ .

### 1. Introduction

Augmentation of heat transfer has been the fundamental subject in the industrial sector that has many thermal applications in heating and cooling. Indeed, the essential problem in such applications is the low thermal conductivity of the traditional fluids such as air, water, and oil. Therefore, the scientific research has found that the main two important techniques of enhancing the low thermal conductivity of the conventional fluids are by using nanoparticles dispersed in the fluids and/or filling the applied regions by porous materials. The idea of using the former technique might be initiated in the beginning of the last century and has become recently more influential with the development of nanotechnology. Consequently, huge studies have been performed about nano-fluids application, for example [1–14] for most recent investigations. In addition, the later technique, which is the use of a mixture of fluid and porous medium, can raise the incorporated thermal conductivity, consequently boosting the aggregate capacity of heat transfer. However, the porous medium used sometimes block the fluid flow within it depending on the porosity and permeability, resulting in a reduction in the convective heat transfer. Therefore, the choice of a porous medium with appropriate thermal and physical properties for

heat augmentation is an essential issue.

Mixed convective flow throughout rectangular or square enclosures filled with saturated porous media has a crucial importance in many practical thermal implementations as for example electronic heat exchangers packed with micro-pin-fin or micro-spheres and exposed to cooled currents. Indeed, in mixed convective flows, the main driving forces namely; the buoyancy forces as a result of the temperature gradients and the shear forces due to the mechanical inlet movement, can result in different complicated flow and thermal behaviours in enclosures due to the changes in their relative action directions and relative magnitudes. For instance, relying on the comparative orientation of the buoyant flow to that of the shearing flow, the buoyant flow can be assisted or hindered to it, changing the direction of the main flow and motivating an enhancement or a diminution in heat transfer. Enormous numerical studies have been published in the last several years onto the case of a lid-driven mixed convective flows in porous enclosures. Khanafer and Chamkha [15], Al-Amiri [16] and Khanafer and Vafai [17] investigated the fluid flow and thermal behaviours of mixed convection in a lid-driven cavity packed by a porous material, with boundaries so the top lid is moving and the vertical walls provide a horizontal temperature gradient, are applied. Khanafer and Chamkha [15] reported that the existence of the porous material restrains significantly the

\* Corresponding author at: Workshop and Training Centre, University of Technology, Baghdad, Iraq.

E-mail addresses: [20046@uotechnology.edu.iq](mailto:20046@uotechnology.edu.iq) (W.H. Alawee), [gazy.alsumaily@monash.edu](mailto:gazy.alsumaily@monash.edu) (G.F. Al-Sumaily), [10592@uotechnology.edu.iq](mailto:10592@uotechnology.edu.iq) (H.A. Dhahad), [mark.thompson@monash.edu](mailto:mark.thompson@monash.edu) (M.C. Thompson).

<https://doi.org/10.1016/j.tsep.2021.100922>

**Nomenclature**

$C_F$	inertia coefficient.
$c_p$	specific heat capacity, $(J/(kg.C^{\circ}))$ .
$d$	inlet/outlet opening width, $(m)$ .
$Da$	Darcy number, $(K/H^2)$ .
$g$	gravitational acceleration.
$Gr$	Grashof number, $Gr = g\beta.H^3.(T_h - T_o)/\nu^2$ .
$h_x$	local convective heat transfer coefficient, $(W/m^2.K)$ .
$H$	enclosure length, $(m)$ .
$k$	thermal conductivity, $(W/m.K)$ .
$K$	permeability, $(s/m)$ .
$K_r$	solid-to-fluid thermal conductivity ratio, $(k_f/k_s)$ .
$Nu_l$	local Nusselt number.
$Nu_m$	mean Nusselt number.
$p$	pressure, $(N/m^2)$ .
$P$	non-dimensional pressure, $P = p/\rho.v_o^2$ .
$Pr$	fluid Prandtl number, $Pr = \nu_f/\alpha_f = 0.71$ for air..
$Re$	Reynolds number, $Re = v_o.H/\nu$ .
$Ri$	Richardson number, $Ri = Gr/Re^2$ .
$T$	temperature, $(C^{\circ})$ .
$t$	time, $(sec)$ .
$u$	flow velocity in x-direction, $(m/s)$ .
$U$	non-dimensional velocity in X-direction, $U = u/v_o$ .
$v$	flow velocity in y-direction, $(m/s)$ .

$V$	non-dimensional velocity in Y-direction, $V = v/v_o$ .
$x, y$	Coordinates, $(m)$ .
$X, Y$	non-dimensional coordinates, $X = x/H, Y = y/H$ .

**Greek symbols**

$\alpha$	thermal diffusivity.
$\beta$	coefficient of volumetric expansion.
$\theta$	non-dimensional temperature, $\theta = (T - T_o)/(T_h - T_o)$ .
$\rho$	density, $(kg/m^3)$ .
$\epsilon$	porosity.
$\mu$	dynamic viscosity, $(N.s/m^2)$ .
$\nu$	kinematic viscosity, $(m^2/s)$ .
$\tau$	non-dimensional time.

**Subscripts**

eff	effective.
f	fluid.
h	hot.
l	local.
m	mean.
n	perpendicular.
o	inlet.
s	solid.
w	wall.

convective currents. Also, the existence of the interior heat generation impacts considerably the temperature distribution; however, it does not affect the flow behaviour very much for small Richardson numbers. Al-Amiri [16] also reported that the existence of porous materials increases clearly the stable thermal stratification in the enclosure, and then restrains the convective flow motion. Moreover, the increase in Darcy number stimulates substantially the activity of the fluid flow, consequently augmenting the convection heat transfer. Khanafer and Vafai [17] found a higher repression in the convective flow currents at higher Lewis number.

Oztop [18] studied numerically mixed convection in a lid-driven porous enclosure partially heated by a finite-length heat element. The top cover is moving horizontally in a one direction, i.e. from left to right, with a fixed temperature and velocity boundary conditions. It was indicated that the cavity structure with a finite-length source of heat positioned on the vertical left wall has the preferable situation for better heat transfer. Jeng and Tzeng [19] investigated numerically mixed convective fluid flow and heat transfer in a lid-driven square enclosure occupied with a water-saturated aluminium fibrous foam, with a moving upper-cooled horizontal surface and a fixed lower-heated horizontal surface. They analysed the effects of the foam porosity, the Reynolds number, and the Grashof number on the flow behaviour and thermal performance in the porous enclosure. Their results showed that using a bigger porosity induces far more augmentation in convection heat removal; however, a lesser porosity is required for larger aggregate heat discharge as a consequence of the high enhancement in the value of effective thermal conductivity. Vishnuvardhanarao and Das [20] analysed numerically mixed convective flow behaviour in an enclosure stuffed with a Darcian porous medium. Both the right and left walls are assumed to be moving upward with similar velocity, and they are kept at hot and cold fixed temperatures, respectively. Whereas, the other two horizontal boundaries are assumed to be thermally isolated. They also reported a significant suppression for the convective currents due to the existing of the porous medium. They indicated that as Richardson number increases, the average Nusselt number approaches a value of one, asymptotically for a Grashof number of  $10^2$ ; however, for a Grashof number of  $10^4$ , an asymptotic value of 1.5 is acquired.

Basak et al. [21] examined numerically the effect of uniform heating of bottom surface on mixed convective flows in a lid-driven enclosure packed with a porous material, for two boundary conditions; vertical side walls being linearly heated and only the vertical right side wall being cooled. The top horizontal lid is isolated and set to a constant velocity. Interestingly, they observed oscillations in the mean Nusselt number on the sidewalls as Reynolds number reaches to the value of ten owing to forming of multiple circulation cells. Ahmed [22] studied mixed convective flow in a double-side lid-driven cavity saturated with a non-Darcy porous material. The lower surface is cooled, whereas the upper surface is consistently heated, and both are mobile in opposing directions, while the vertical sidewalls are maintained thermally insulated. The results revealed that as the inverse Darcy number increases, a considerable reduction in the thermal boundary layer is developed, leading to a clear decrease in Nusselt number. Also, it was found that the raising in Richardson number causes a stable thermal stratification in the enclosure producing a reduction in Nusselt number. The mean Nusselt number was reported to reduce as either Prandtl number or the thermal conductivity ratio increases. Wang and Qin [23] investigated non-Darcy mixed convective flow in a double lid-driven porous cavity by moving the horizontal lids in opposite directions with two heat sources in the middle of the drying chamber. The results revealed a significant enhancement in heat, flow, and mass transfer within the enclosure with amplification in Darcy and/or Richardson numbers. Wang et al. [24] examined the influence of thin porous fins on mixed convective flow and thermal characteristics in a lid-driven enclosure with the upper surface being moving in the two-ways. The porous fins are attached to the vertical left wall, and both vertical sidewalls are maintained at fixed but diverse temperatures, whereas the horizontal surfaces are thermally isolated. The results showed that the heat transfer augmentation as a result of increasing Darcy number at first grows, and then slowly diminishes, and the same trend was found for the effect of porous fins numbers.

However, the problem of mixed convection flow and heat transfer within a ventilated rectangular or square cavity packed with a porous material has been received relatively much less attention in the literature. Mahmud and Pop [25] analysed numerically steady Darcian mixed

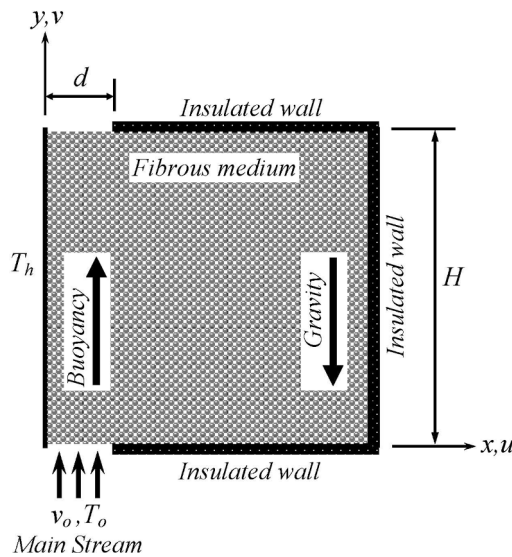


Fig. 1. Physical configuration.

convective flow during a ventilated cavity stuffed with a porous material, with the left side wall being isothermally heated and the other three walls being isolated. They reported that the flow model could transform from a unicellular flow to a multi-cellular one by the variation of the govern parameters such as Péclet and Rayleigh numbers and the inlet opening size. They also found that the rates of heat transfer are most sensitive to the alteration in the inlet opening size. Murthy and Kumar [26] tested the influence of non-isothermal heating and the suction/injection effects at bottom/top or top/bottom walls on non-Darcian convective flow in a square porous cavity. Results were reported for various parameters such as Rayleigh number, Grashof number, the suction/injection port size, the inlet suction/injection velocity, and the amplitude of the boundary sinusoidal temperature profile. The results showed that interesting multi-cellular circulation cells caused by the complicated alterations in the flow pattern are stimulated in the cavity. In addition, it was found that Nusselt numbers, and temperature and flow fields are very much responsive to every one of the aforementioned controlling parameters.

Kumar and Murthy [27] and Murthy and Kumar [28] studied mixed convective flows in vertical cavities packed with a Darcian and non-Darcian porous materials, respectively, with multiple suction/injection effects, with a vertical left wall being isothermally heated to stimulate the natural convection. The results obtained revealed that the rates of heat transfer from the heated wall decline with increasing the suction/injection velocities; however, they increase with increasing the suction/injection openings and Rayleigh number. Behzadi et al. [29] investigated numerically the impact of adding spherical beads as a porous medium inside a vented square horizontal cavity on the rates of Darcian mixed convection heat transfer. A constant heat flux is supplied along the horizontal bottom surface for cavity heating, while the top surface is maintained at a constant temperature, and the other left and right sides are adiabatic. The effects of Darcy and Richardson numbers and the particle size on the flow behaviour and temperature distribution, were studied. They found that the rates of heat transfer decrease by increasing Darcy number and/or the porous particles diameters.

Once again, the above literature reveals that the case of mixed

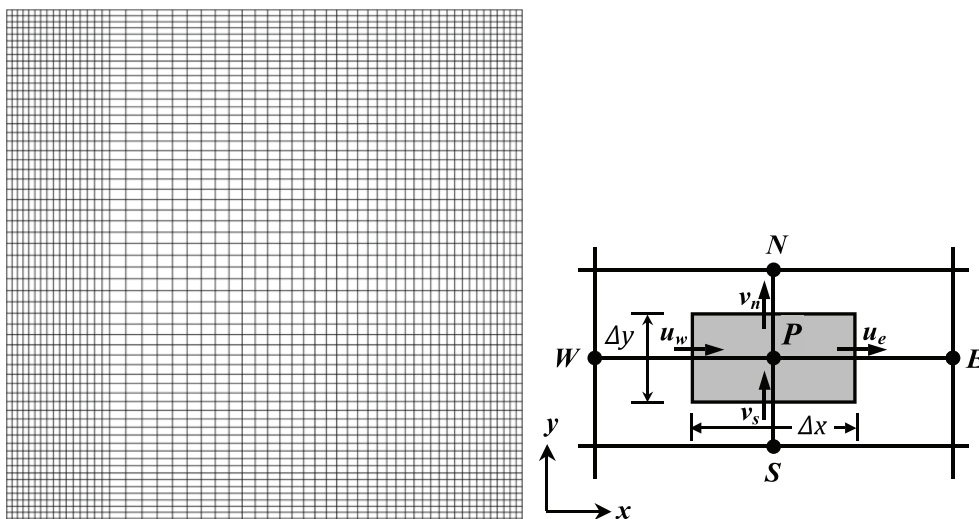


Fig. 2. (Left) Computational grid, (Right) Conventional control volume demonstrating the main grid nodes and the staggered locations.

**Table 1**

Grid sizes used to check the grid independency.

mesh	( $\Delta x \times \Delta y$ )
M1	(31 × 31)
M2	(41 × 41)
M3	(51 × 51)
M4	(61 × 61)
M5	(71 × 71)
M6	(81 × 81)

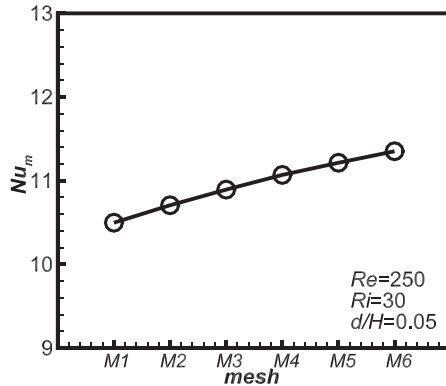


Fig. 3. Results of  $Nu_m$  for the grid resolution study.

convection inside a porous enclosure vertically ventilated has not been thoroughly researched, especially when taking the non-Darcian effects into consideration. Therefore, the current study reports detailed results about the thermal performance within such a porous system for more valuable understanding. It is worth indicating that the current case was recently studied by Dhahad et al. [30] dealing with the similar vented enclosure but without porous media. The attention is focused on the effects of different pertinent parameters such as Richardson number, Reynolds number, Darcy number, the solid/fluid thermal conductivity ratio, the porosity, and the inlet/outlet port width, on the transient mixed convective flow and thermal characteristics. Thus, fluid flow and temperature distributions are also presented and analysed by tracing streamlines and isotherms within the enclosure.

## 2. Physical problem and Mathematical Formulation

The present study considers a vertical square cavity with a length of  $H$ , stuffed with a non-Darcian fibrous porous material, and heated along the left vertical wall at a fixed temperature,  $T_h$ , and the other boundaries being completely insulated. Thus, the temperature gradient is acting in the horizontal direction. Whereas, an airflow enters the enclosure from the bottom surface, adjacent the lower edge of the vertical left wall by the effect of a vertical forced pressure, at a velocity  $v_o$  and a temperature  $T_o$ , and exits it from the top surface in the opposite edge, as demonstrated in Fig. 1, where,  $d$  refers to the inlet/outlet widths. Thus the heat is lost by convection and conduction from the hot wall to the flowing fluid and the solid porous matrix, respectively, and then is exposed to the environment by the outlet vent. Therefore, the temperature discrepancy between the hot wall and the through-stream close to it stimulates the buoyancy effects. For the porous medium occupied the enclosure, the following assumptions are considered: the stationary solid porous material and the mobile fluid are in local thermal equilibrium; the inertia forces and the viscous drag effect of the porous solid matrix in momentum equations are not neglected, e.g. non-Darcian model; the properties of the porous medium and the fluid are fixed, except the fluid density variation, which obeys the Boussinesq approximation. The airflow is presumed to be unsteady, laminar, two-dimensional, newtonian, and incompressible. The gravitational

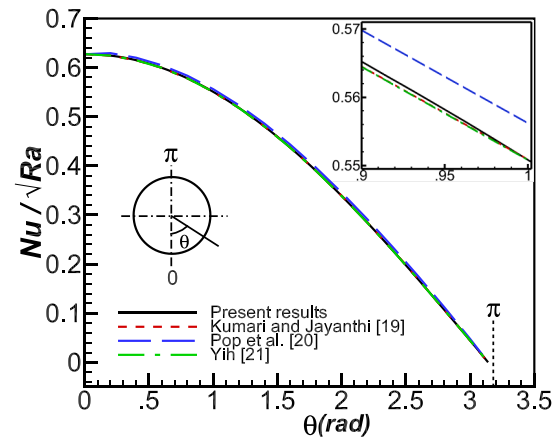


Fig. 4. Local Nusselt number  $Nu/\sqrt{Ra}$  along the cylinder perimeter for our code, Kumari and Jayanthi [35], Pop et al. [36], and Yih [37].

acceleration operates in the negative y-direction, opposite to the action direction of the buoyancy forces. Subject to these assumptions, the equations of continuity, full-momentum, and one-energy, can be denoted in the following dimensional format (Kaviany [31] and Nield and Bejan [32]):

$$\frac{\partial u}{\partial x} + \frac{\partial v}{\partial y} = 0, \tag{1}$$

$$\frac{\rho_f}{\varepsilon} \left( \frac{\partial u}{\partial t} \right) + \frac{\rho_f}{\varepsilon^2} \left( u \frac{\partial u}{\partial x} + v \frac{\partial u}{\partial y} \right) = -\frac{\partial p}{\partial x} + \frac{\mu_f}{\varepsilon} \left( \frac{\partial^2 u}{\partial x^2} + \frac{\partial^2 u}{\partial y^2} \right) + S_u, \tag{2}$$

where,

$$S_u = -\frac{\mu_f}{K} u - \frac{\rho_f C_F \varepsilon}{\sqrt{K}} |\mathbf{u}| u,$$

**Table 2**

Thermal conductivities for some metallic and non-metallic materials, and their ratios to air thermal conductivity  $k_f = 0.02587 \text{ W/m.K}$  at  $20^\circ\text{C}$  as a working fluid.

Metallic materials	$k_s$ (W/m.K at $20^\circ\text{C}$ )	$K_r$
silver	429	$1.658 \times 10^4$
copper	385	$1.488 \times 10^4$
aluminium	237	$9.161 \times 10^3$
bronze	189	$7.305 \times 10^3$
brass	144	$5.566 \times 10^3$
iron	79	$3.053 \times 10^3$
nickle	62	$2.396 \times 10^3$
steel	50	$1.932 \times 10^3$
lead	35	$1.352 \times 10^3$
Non-metallic materials	$k_s$ (W/m.K at $20^\circ\text{C}$ )	$k_r$
carbon	6.92	$2.674 \times 10^2$
window glass	1.0	$0.386 \times 10^2$
concrete	0.8	$0.309 \times 10^2$
soil	0.5	$0.193 \times 10^2$
brick	0.47	$0.181 \times 10^2$
crystal	0.2	$0.773 \times 10^1$
wood	0.17	$0.657 \times 10^1$
rubber	0.138	$0.533 \times 10^1$
foam	0.026	$1.005 \times 10^0$

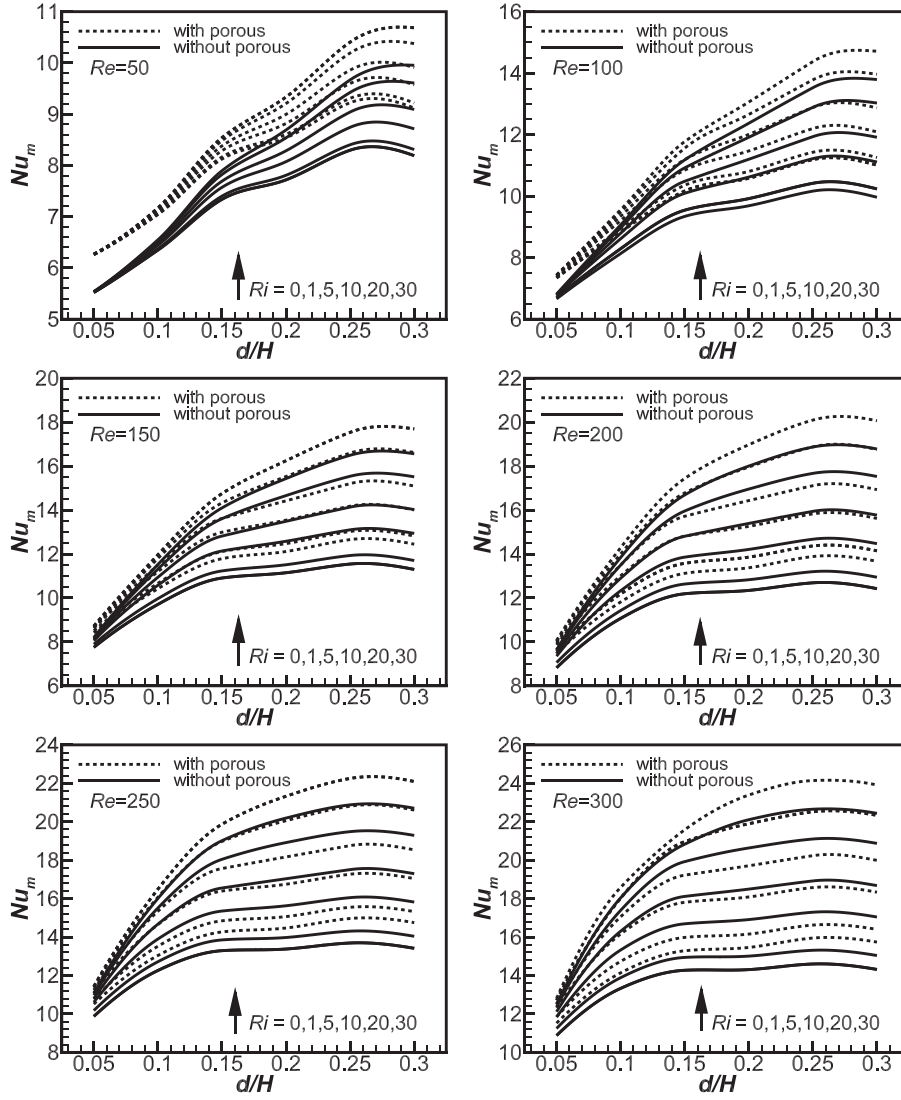


Fig. 5. Mean Nusselt number  $Nu_m$  with  $d/H$  at different  $Re$  and  $Ri$ , without a porous medium, and with a porous medium at  $\varepsilon = 0.95$ ,  $Da = 0.1$  and  $K_r = 1000$ .

$$\frac{\rho_f}{\varepsilon} \left( \frac{\partial v}{\partial t} \right) + \frac{\rho_f}{\varepsilon^2} \left( u \frac{\partial v}{\partial x} + v \frac{\partial v}{\partial y} \right) = - \frac{\partial p}{\partial y} + \frac{\mu_f}{\varepsilon} \left( \frac{\partial^2 v}{\partial x^2} + \frac{\partial^2 v}{\partial y^2} \right) + S_v + \rho_f \beta_f g (T - T_o), \quad (3)$$

where,

$$S_v = - \frac{\mu_f}{K} v - \frac{\rho_f C_F \varepsilon}{\sqrt{K}} |\vec{u}| v,$$

here,

$$|\vec{u}| = \sqrt{u^2 + v^2},$$

$$(\rho c_p)_m \left( \frac{\partial T}{\partial t} \right) + \varepsilon (\rho c_p)_f \left( u \frac{\partial T}{\partial x} + v \frac{\partial T}{\partial y} \right) = \left[ \frac{\partial}{\partial x} \left( k_{f,eff} \frac{\partial T}{\partial x} \right) + \frac{\partial}{\partial y} \left( k_{f,eff} \frac{\partial T}{\partial y} \right) \right], \quad (4)$$

where,

$$(\rho c_p)_m = \varepsilon (\rho c_p)_f + (1 - \varepsilon) (\rho c_p)_s,$$

where,  $u$  and  $v$  are the flow velocity components in the pore scale in  $x$

and  $y$  directions, respectively. Also,  $t$  represents the time variable,  $p$  and  $T$  represent the fluid pressure and temperature fields, respectively, while,  $\rho_f$ ,  $\mu_f$  and  $k_{f,eff}$  refer to the density, dynamic viscosity, and effective thermal conductivity, respectively, of the fluid. Moreover,  $c_p$  is the specific heat,  $C_F$ ,  $K$ , and  $\varepsilon$  are the inertia coefficient, the permeability, and the porosity of the porous medium, respectively. The subscripts  $f$  and  $s$  refers to the fluid and solid phases, respectively. To assess the fluid velocity and temperature fields in the porous medium in a general scale, the following non-dimensional scaling parameters are used:

$$U = \frac{u}{v_o}, \quad V = \frac{v}{v_o}, \quad X = \frac{x}{H}, \quad Y = \frac{y}{H}, \quad P = \frac{p}{\rho v_o^2}, \quad \tau = \frac{t}{v_o H}, \quad \theta = \frac{T - T_o}{T_h - T_o}, \quad (5)$$

where,  $\rho v_o^2$  is the characteristic pressure. By substituting the parameters in Eq. (5) into the above-mentioned equations (1)–(4), the following dimensionless formulations are produced:

$$\frac{\partial U}{\partial X} + \frac{\partial V}{\partial Y} = 0, \quad (6)$$

$$\left( \frac{\partial U}{\partial \tau} \right) + \frac{1}{\varepsilon} \left( U \frac{\partial U}{\partial X} + V \frac{\partial U}{\partial Y} \right) = - \varepsilon \left( \frac{\partial P}{\partial X} \right) + \frac{1}{Re} \left( \frac{\partial^2 U}{\partial X^2} + \frac{\partial^2 U}{\partial Y^2} \right) + S_U, \quad (7)$$

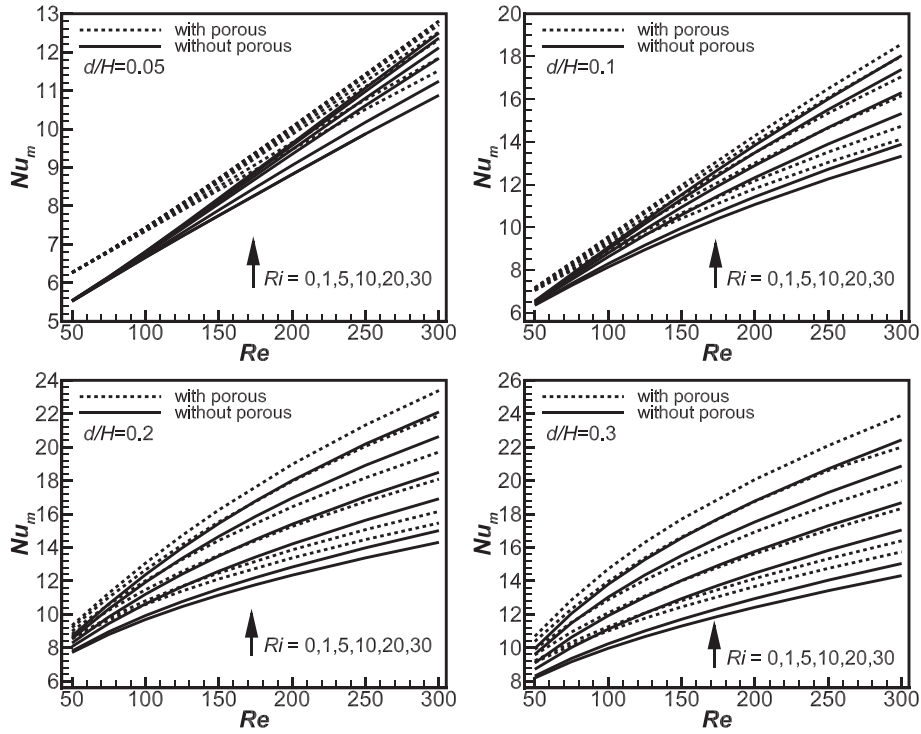


Fig. 6. Mean Nusselt number  $Nu_m$  with  $Re$  at different  $Ri$  and  $d/H$ , without a porous medium, and with a porous medium at  $\epsilon = 0.95$ ,  $Da = 0.1$  and  $K_r = 1000$ .

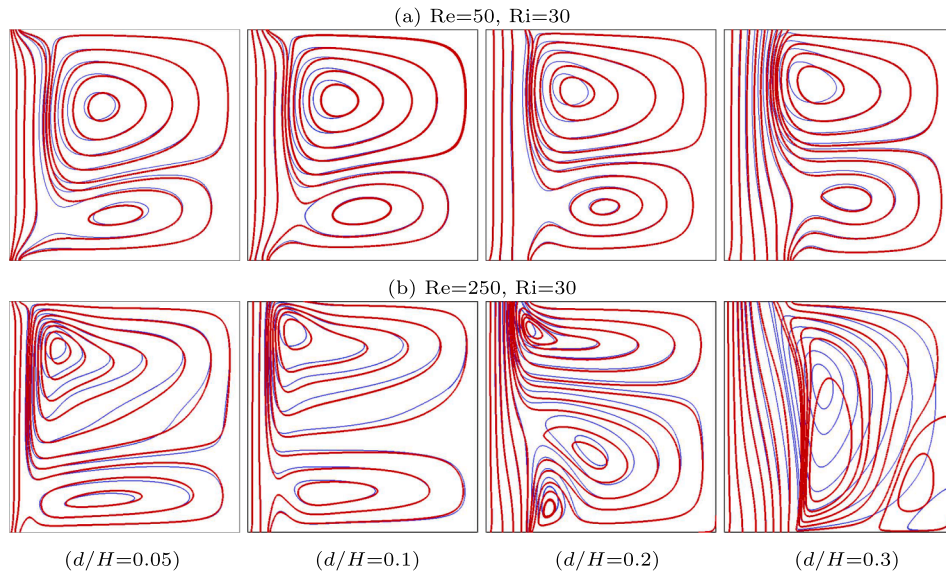


Fig. 7. Streamlines patterns for (a)  $Re = 50$ ,  $Ri = 30$  and (b)  $Re = 250$ ,  $Ri = 30$ , at  $d/H$  changing over (0.05–0.3). (Blue) without porous and (Red) with porous at  $\epsilon = 0.95$ ,  $Da = 0.1$  and  $K_r = 1000$ . (For interpretation of the references to color in this figure legend, the reader is referred to the web version of this article)

where,

$$S_U = -\frac{\epsilon}{Re \cdot Da} U - \frac{\epsilon^2 \cdot C_F}{\sqrt{Da}} |\vec{U}| U,$$

$$\left(\frac{\partial V}{\partial \tau}\right) + \frac{1}{\epsilon} \left( U \frac{\partial V}{\partial X} + V \frac{\partial V}{\partial Y} \right) = -\epsilon \left( \frac{\partial P}{\partial Y} \right) + \frac{1}{Re} \left( \frac{\partial^2 V}{\partial X^2} + \frac{\partial^2 V}{\partial Y^2} \right) + S_V + \epsilon Ri \theta, \tag{8}$$

where,

$$S_V = -\frac{\epsilon}{Re \cdot Da} V - \frac{\epsilon^2 \cdot C_F}{\sqrt{Da}} |\vec{U}| V,$$

and,

$$|\vec{U}| = \sqrt{U^2 + V^2},$$

$$C_F = \frac{1.75}{\sqrt{150 \epsilon^3}},$$

$$\left(\frac{\partial\theta}{\partial\tau}\right) + \frac{\varepsilon}{C} \left( U \frac{\partial\theta}{\partial X} + V \frac{\partial\theta}{\partial Y} \right) = \frac{1}{C \cdot \text{Re} \cdot \text{Pr}} \left[ \frac{\partial}{\partial x} \left( k_{f,\text{eff}} \frac{\partial\theta}{\partial x} \right) + \frac{\partial}{\partial y} \left( k_{f,\text{eff}} \frac{\partial\theta}{\partial y} \right) \right], \quad (9)$$

where,

$$k_{f,\text{eff}} = \frac{k_{st}}{k_f} = (1 - \sqrt{1 - \varepsilon}) + \frac{2\sqrt{1 - \varepsilon}}{1 - \lambda B} \times \left[ \frac{(1 - \lambda)B}{(1 - \lambda B)^2} \ln(\lambda B) - \frac{B + 1}{2} - \frac{B - 1}{1 - \lambda B} \right], \quad (10)$$

where,

$$\lambda = 1 / K_r, \quad B = 1.25[(1 - \varepsilon)/\varepsilon]^{10}, \quad C = \varepsilon + (1 - \varepsilon) \left( \frac{k_r}{\alpha_r} \right),$$

where,  $U, V$  represent the dimensionless velocity components in the pore scale along the dimensionless directions  $X$  and  $Y$ , respectively; while  $P, \theta$ , and  $\tau$  denote to the dimensionless pressure, temperature, and time, respectively. The primary parameters that control the current physical case are Reynolds number (Re), Richardson number (Ri), Darcy number (Da), Prandtl number (Pr), and the solid/fluid thermal

conductivity ratio ( $K_r$ ), and can be defined as follows:

$$\text{Re} = \frac{\nu_o \rho_f H}{\mu_f}, \quad \text{Ri} = \frac{\text{Gr}}{\text{Re}^2}, \quad \text{Da} = \frac{K}{H^2}, \quad \text{Pr} = \frac{\nu_f}{\alpha_f}, \quad K_r = \frac{k_s}{k_f}, \quad (11)$$

where, Gr is the Grashoff number as follows:

$$\text{Gr} = \frac{g \cdot \beta_f \cdot \rho_f^2 \cdot H^3 (T_h - T_o)}{\mu_f^2}, \quad (12)$$

here,  $\nu_f$  and  $\alpha_f$  are the momentum diffusivity (kinematic viscosity) and the thermal diffusivity, respectively, of the fluid. Dirichlet boundary conditions for the pertinent variables, i.e. the velocities and the temperature, are imposed on the inlet, while Neumann boundary conditions are imposed at the outlet and solid boundaries. Thus, the non-dimensional initial and boundary conditions applied in the present case can be specified as follows:

$$\begin{aligned} U = V = \theta = 0, & \quad \text{everywhere in the domain at } \tau = 0. \\ \text{at inlet slot, } & U_o = 0, V_o = -1, \theta_o = 0, \\ \text{at exit vent, } & \partial U / \partial Y = \partial V / \partial Y = \partial \theta / \partial Y = 0, \\ \text{at vertical left wall, } & U_h = 0, V_h = 0, \theta_h = 1, \\ \text{at other walls, } & U = V = 0, \partial \theta / \partial (X, Y) = 0. \end{aligned} \quad (13)$$

The heat transfer occurred between the vertical hot wall and the air

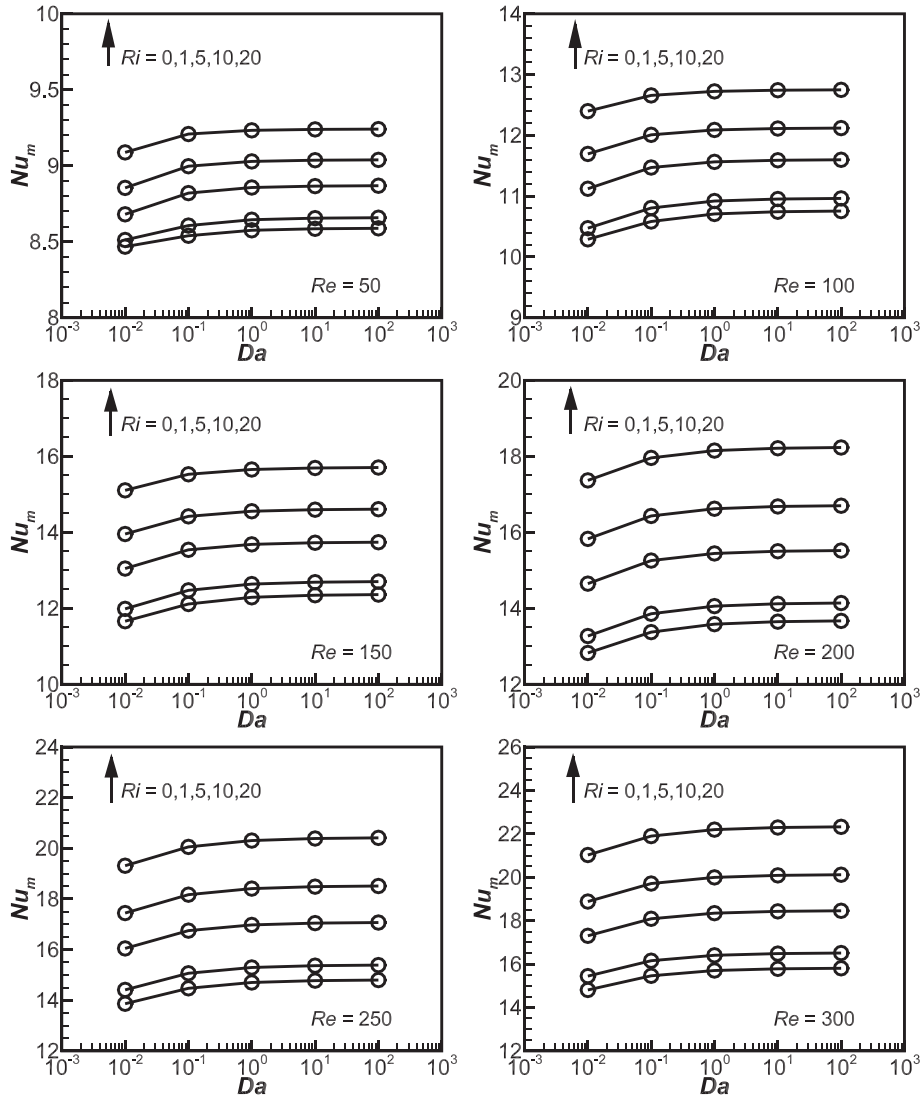


Fig. 8. Mean Nusselt number  $Nu_m$  with  $Da$  for different  $Re$  and  $Ri$ , at  $d/H = 0.2$ ,  $\varepsilon = 0.95$  and  $K_r = 1000$ .

flowing nearby is calculated in relation of the local Nusselt number ( $Nu_l$ ) by the following formula:

$$Nu_l = \frac{h_x \cdot Y}{k_f} = \frac{-k_{f,eff} \cdot (\partial T / \partial n) \cdot Y}{k_f \cdot (T_h - T_o)} = \frac{-k_{f,eff} \cdot \partial \theta}{k_f \cdot \partial n} \Big|_h, \quad (14)$$

here  $h_x$  is the local convective heat transfer coefficient in  $X$  direction, perpendicular  $n$  to the vertical hot wall. Then, the mean Nusselt number ( $Nu_m$ ) can be calculated by integrating  $Nu_l$  along the hot wall as follows:

$$Nu_m = \frac{1}{H} \sum \int_0^H Nu_l \cdot dn \quad (15)$$

### 3. Numerical procedure

The non-dimensional highly coupled governing Eqs. (6)–(9), describing the evolution of momentum and energy transport in unsteady mixed convective flow, need to be discretised numerically in both space and time. Therefore, the finite volume method developed by Patankar [33] was incorporated and employed in an in-house FORTRAN program

to numerically discretise and solve the aforementioned equations, and simulate the velocity, pressure, and temperature fields inside the porous enclosure. Firstly, the computational domain is entirely divided into non-uniformly spaced grid lines in both horizontal and vertical directions, as demonstrated in Fig. 2(Left). Indeed, the spacing of the computational grid is generated non-uniformly in the areas that undergo high sharp gradients in particular inlet, outlet, and near to walls. The main grid horizontal lines are intersected with those in vertical direction forming so-called grid nodes during the domain. These nodes are presumed to be enclosed with imaginary control volumes. Hence, each control volume surrounds a typical node  $P$ , which has boundaries that are considered to be in the mid-way between the neighbouring grid north  $N$ , south  $S$ , east  $E$ , and west  $W$  nodes. The entire scalar variables, in particular temperature and pressure, are reserved in the main grid points, whereas the vector variables namely, velocity components, are reserved at the boundaries of the control volumes. Indeed, these boundary locations are commonly called staggered locations, and forming what is called a staggered grid for storing velocity components. The appropriation such staggered locations beside the main grid points

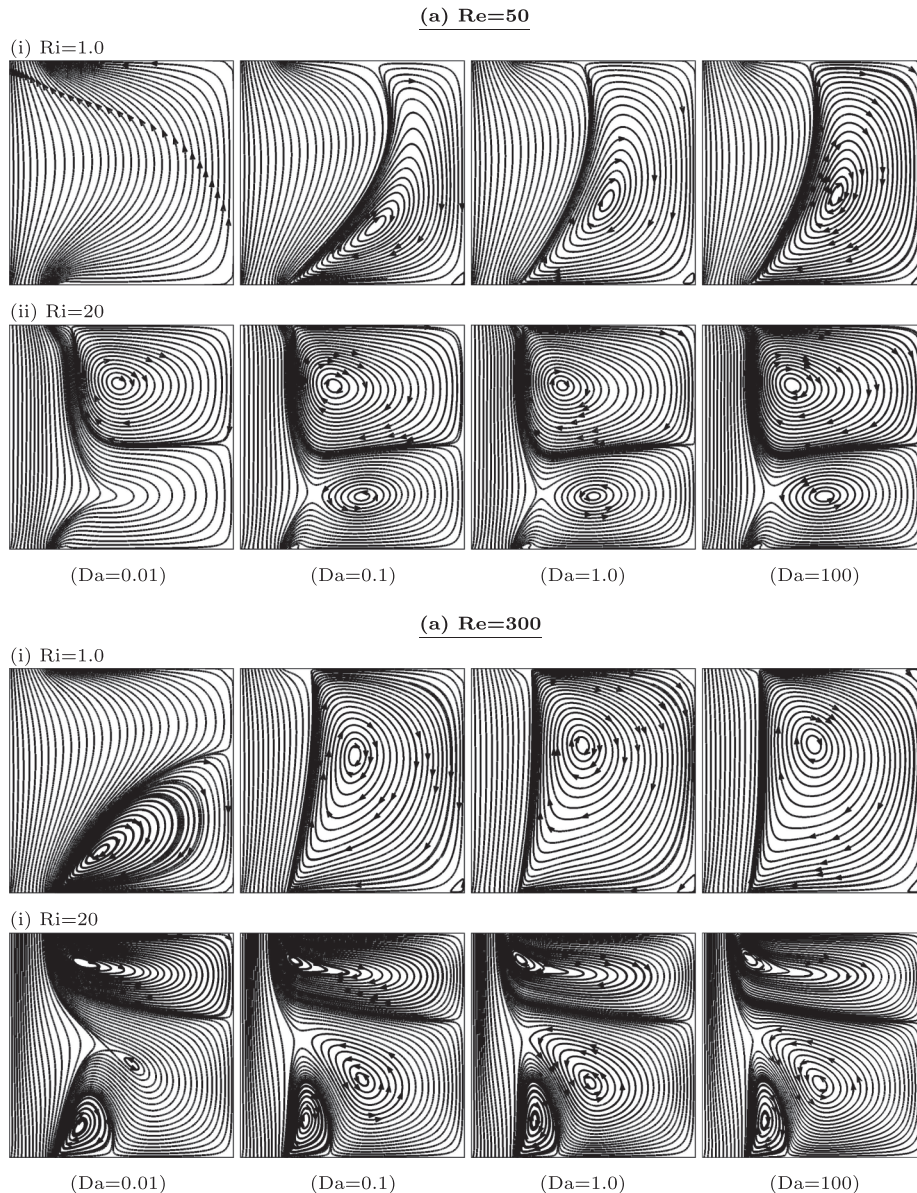


Fig. 9. Streamlines patterns for different  $Da$  (0.01–100), at (a)  $Re = 50$  and (b)  $Re = 300$ , for (i)  $Ri = 1.0$  and (ii)  $Ri = 20$ , at  $d/H = 0.2$ ,  $\epsilon = 0.95$  and  $K_r = 1000$ .

secures that the velocities situated between the pressures that stimulate them, and are accessible straightforward for calculating the fluxes of convection of the scalar variables. Fig. 2(Right) shows a conventional finite control volume with dimensions  $(\Delta x \times \Delta y)$  about a typical grid node P being in communication with the four adjacent grid nodes N, S, E, W, as well as the staggered positions for storing the velocities at the four boundaries of the control volume. After that, the governing differential Eqs. (6)–(9) are mathematically integrated across the finite control volume utilising the Hybrid differencing scheme reported in Ferziger and Peric [34] for formulating non-linear algebraic approximations. Then, the SIMPLEC algorithm of Patankar [33] is used to connect the continuity and the momentum approximations, and solve them iteratively throughout the entire control volumes employing the alternating direction implicit (ADI) technique, and estimating the values of the pertinent variables at the whole grid nodes. After each a complete numerical iteration, assessment for the accuracy of the calculated results is conducted. This is done by verifying adequately diminutive residuals for all dependent variables estimated all over the computational domain, are diminished to a satisfactory standard level, utilising a convergence criteria. In the current investigation, the estimated local and mean Nusselt numbers  $Nu_l$  and  $Nu_m$  are monitored as an accuracy indication for the convergence of the numerical solution. The value of convergence criteria employed is generally less than  $(10^{-6})$ .

A grid resolution study is conducted to assure that the numerical results are independent to the computational grid employed. Different non-uniform grid sizes  $M1, M2, M3, M4, M5,$  and  $M6$  that are detailed in Table 1, are used. This study is done for several dependent parameters like Richardson number, Reynolds number, and opening size. Fig. 3 illustrates a sample of the study results. The grid size  $M4$  with  $61 \times 61$  grid lines is selected to be relevant for the present investigation. This is due to that it permits an acceptable adjustment between the calculation time cost and the precision of the results obtained with a highest numerical deviation  $< 0.1\%$ . In addition, the present numerical algorithm used in our code is verified with the published results of Kumari and Jayanthi [35], Pop et al. [36] and Yih [37], for natural convection heat transfer about a hot circular cylinder positioned in a porous material. Fig. 4 shows the comparison that depicts an adequate agreement with a highest error  $< 0.05\%$ .

#### 4. Results and discussion

First, in such a cooling system described in Fig. 1, the driving forces of fluid flow comprise the shear forces owing to the forced inflow, and the buoyancy forces owing to the temperature gradients, whereas the interaction between these forces leads to different modes of convective flow, e.g. from a purely free convection flow to a purely forced

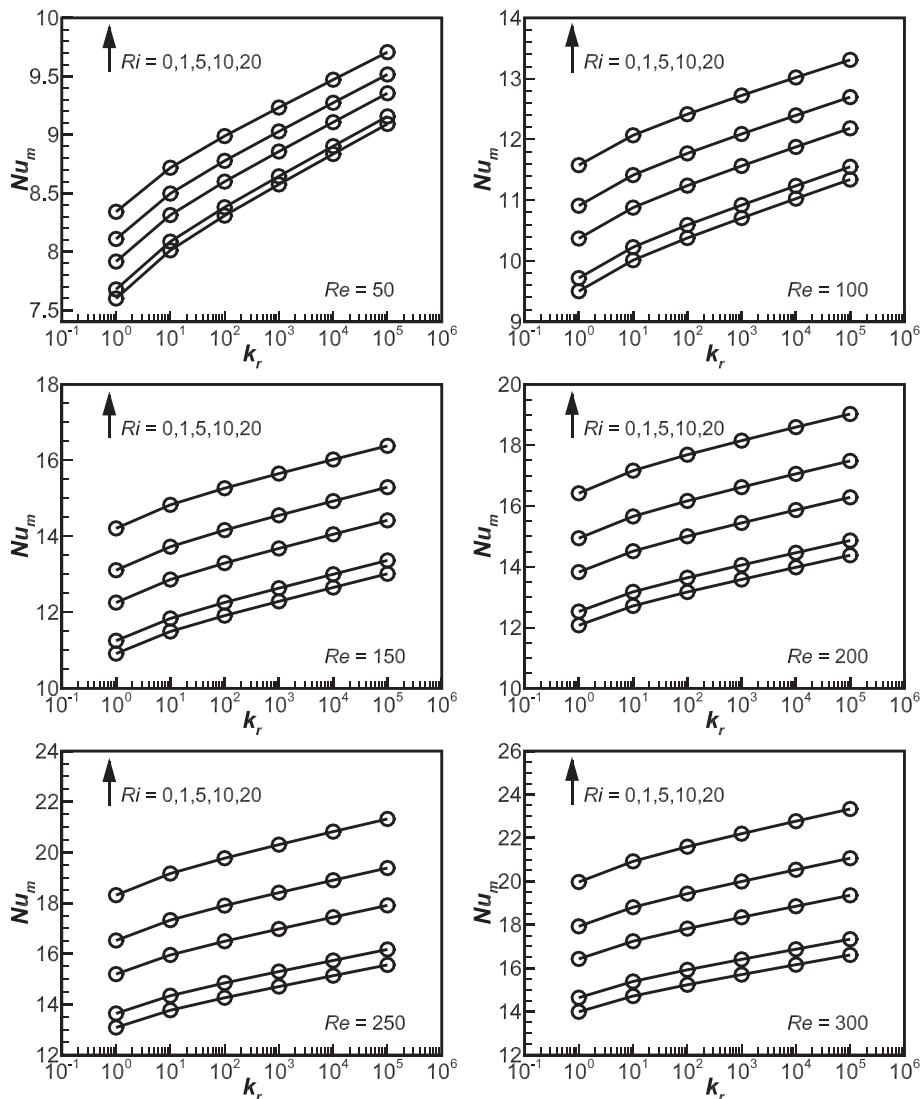


Fig. 10. Mean Nusselt number  $Nu_m$  with  $K_r$  for different  $Re$  and  $Ri$ , at  $d/H = 0.2, \epsilon = 0.95$  and  $Da = 1.0$ .

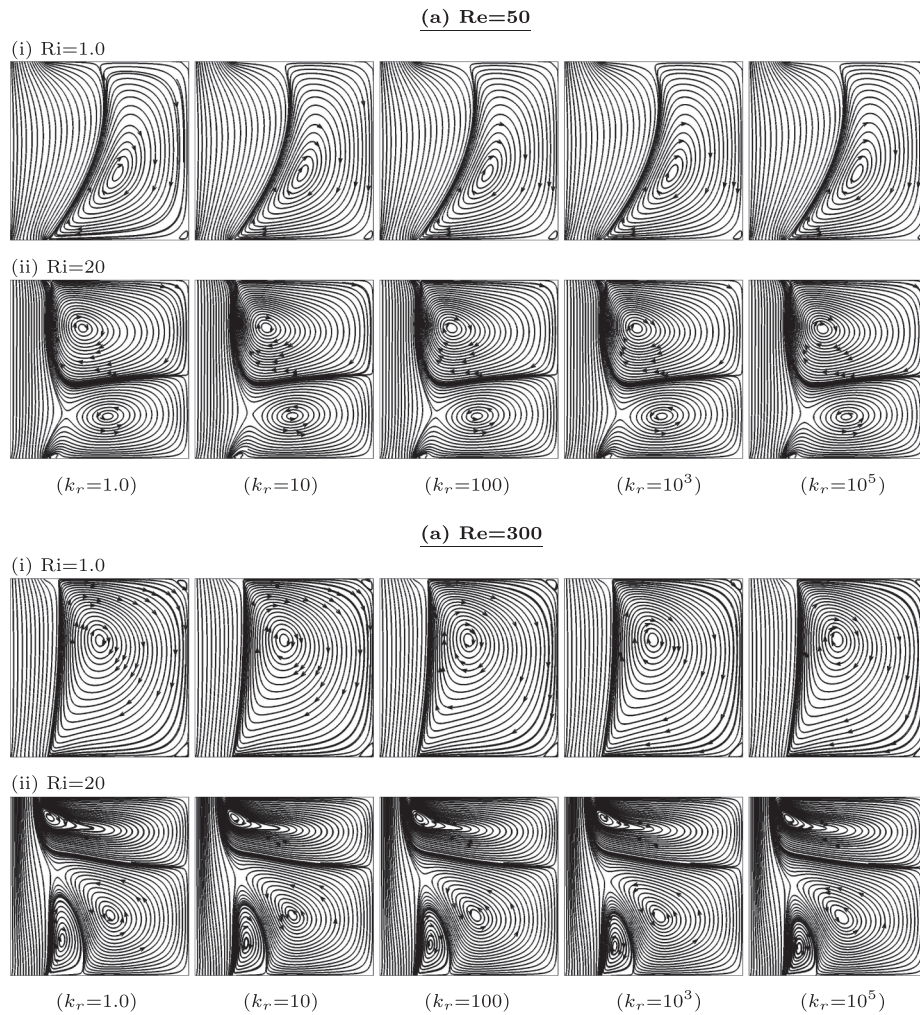
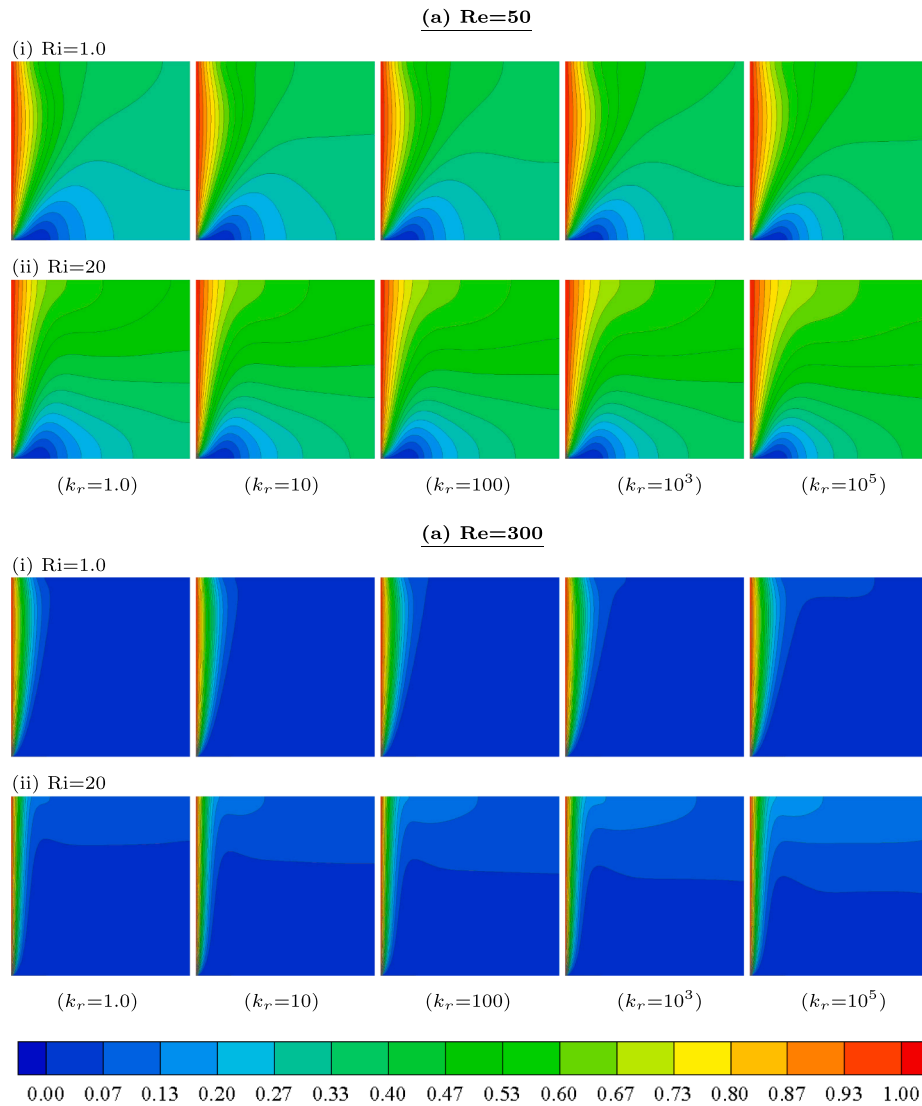


Fig. 11. Streamlines patterns for different  $K_r$  ( $1.0-10^5$ ), at (a)  $Re = 50$  and (b)  $Re = 300$ , for (i)  $Ri = 1.0$  and (ii)  $Ri = 20$ , at  $d/H = 0.2$ ,  $\varepsilon = 0.95$  and  $Da = 1.0$ .

convection. Therefore, the ranges of the main pertinent parameters, which are Reynolds number ( $Re = 50-300$ ) and Richardson number ( $Ri = 0-30$ ), are selected based on the study conducted by Dhahad et al. [30], to cover the mixed convection regime. In addition, the thermal conductivity of metals varies between  $15-450$ , and under this range is for non-metals. The impact of solid/fluid thermal conductivity is investigated within the range of  $K_r = 1-10^5$  to cover a broad range of non-metallic and metallic porous materials, as shown in Table 2.

Fig. 5 illustrates the variation of mean Nusselt number  $Nu_m$  with the opening size ( $d/H = 0.05-0.3$ ), at different Richardson numbers ( $Ri = 0-30$ ) and six selected Reynolds numbers ( $Re = 50, 100, 150, 200, 250, 300$ ), with and without a porous medium. Also, Fig. 6 shows the variation of  $Nu_m$  with Reynolds number ( $Re = 50-300$ ) at different Richardson numbers ( $Ri = 0-30$ ), and at four selected ports sizes ( $d/H = 0.05, 0.1, 0.2, 0.3$ ), with and without a porous medium. The results in these figures are obtained at constant  $Da = 0.1$ ,  $\varepsilon = 0.95$ , and  $K_r = 1000$ . A metallic fibrous material with  $k_s = 26 W/m.K$  can be used for obtaining  $K_r = (k_s/k_f) = 1000$ . Examples of such porous materials are Copper-Bronze alloy (75% Cu, 25% Sn), Copper-German Silver alloy (62% Cu, 15% Ni, 22% Zn) and Steel-Nickel, (10% Ni). It is shown that  $Nu_m$

increases significantly with increasing Reynolds number and/or Richardson number. The reason is due to the thermal dispersion effect, hence, higher Reynolds number or Richardson number generates high-strength convective currents in the enclosure and increases the fluid thermal mixing, which results in bigger  $Nu_m$ . Also,  $Nu_m$  increases as the ports size increases over the entire ranges of Reynolds and Richardson numbers, and its influence becomes more important at greater Richardson numbers. An optimal value of the ports size at  $d/H = 0.25$  is found, for obtaining a peak  $Nu_m$ , hence it is not beneficial to increase the port size after this value. In addition, it is obvious that the presence of the porous medium does not change the trend of  $Nu_m$  with all these parameters; however, it augments the convective heat transfer in general due to the large enhancement in the effective thermal conductivity. Fig. 7 demonstrates the flow streamlines inside the enclosure with a porous medium (Red lines) and without a porous medium (Blue lines), for two cases: (a)  $Re = 50$ ,  $Ri = 30$ , and (b)  $Re = 250$ ,  $Ri = 30$ , for  $d/H$  changing over ( $0.05-0.3$ ). It can be shown that the existence of the porous medium does change the flow behaviour considerably except at high Reynolds numbers and larger ports width. Indeed, in this application, the existing porous material changes only the magnitudes of flow



**Fig. 12.** Isotherms patterns for different  $K_r$  ( $1.0-10^5$ ), at (a)  $Re = 50$  and (b)  $Re = 300$ , for (i)  $Ri = 1.0$  and (ii)  $Ri = 20$ , at  $d/H = 0.2$ ,  $\varepsilon = 0.95$  and  $Da = 1.0$ .

velocity and temperature due to the inclusion of the inertial effects.

Figs. 8 and 9 display the influence of increasing Darcy number on heat transfer and the flow behaviour, at different Reynolds and Richardson numbers, and at constant  $d/H = 0.2$ ,  $\varepsilon = 0.95$  and  $K_r = 1000$ . In these figures, Darcy number, which is straight corresponding to the permeability of the porous medium used, is varied between 0.001–100. One can see that as Darcy number increases, the mean Nusselt number  $Nu_m$  raises markedly. This augmentation in  $Nu_m$  becomes more noticeable for higher Reynolds and Richardsons numbers owing to the more development in the flow fluxes. Also, the increase in the permeability of the porous material generates more thermal energy to be transferred away from the heat source. As shown in Fig. 9 that the raise in the permeability stimulates deeper flow activity in the enclosure, and the decrease in the permeability plays a part into flow repression caused by the stable stratification.

Figs. 10–12 show the effect of varying solid-to-fluid thermal conductivity ratio over the range of ( $K_r = 1-10^5$ ) on  $Nu_m$ , and the flow and

temperature distributions, respectively, for  $Re = 50-300$  and  $Ri = 0-20$ , and at constant  $d/H = 0.2$ ,  $\varepsilon = 0.95$ , and  $Da = 1.0$ . Fig. 10 shows that  $Nu_m$  increases considerably with increasing in the conductivity ratio, for all inflow and heating conditions.

Of course, this is associated with the large temperature gradients generated on the hot wall as a result of the reduction in the fluid thermal boundary layer. Once again, the presence of the porous matrix within the flowing fluid can increase the effective thermal conductivity, Eq. (10), promoting more  $Nu_l$  and  $Nu_m$ , in Eqs. (14) and (15), respectively. Figs. 11 and 12 show that changing the conductivity ratio does not have any observable influence on the flow streamlines. However, the considerable impact of this variable is observed to be on the isotherms patterns. It is shown that the isotherms lines distribute at a greater distance during the entire enclosure as the conductivity ratio raises. Thus, the porous material turns out to be further conductive and the intensity of the convective flow reduces within the porous enclosure, causing the porous matrix approximately isothermal for higher

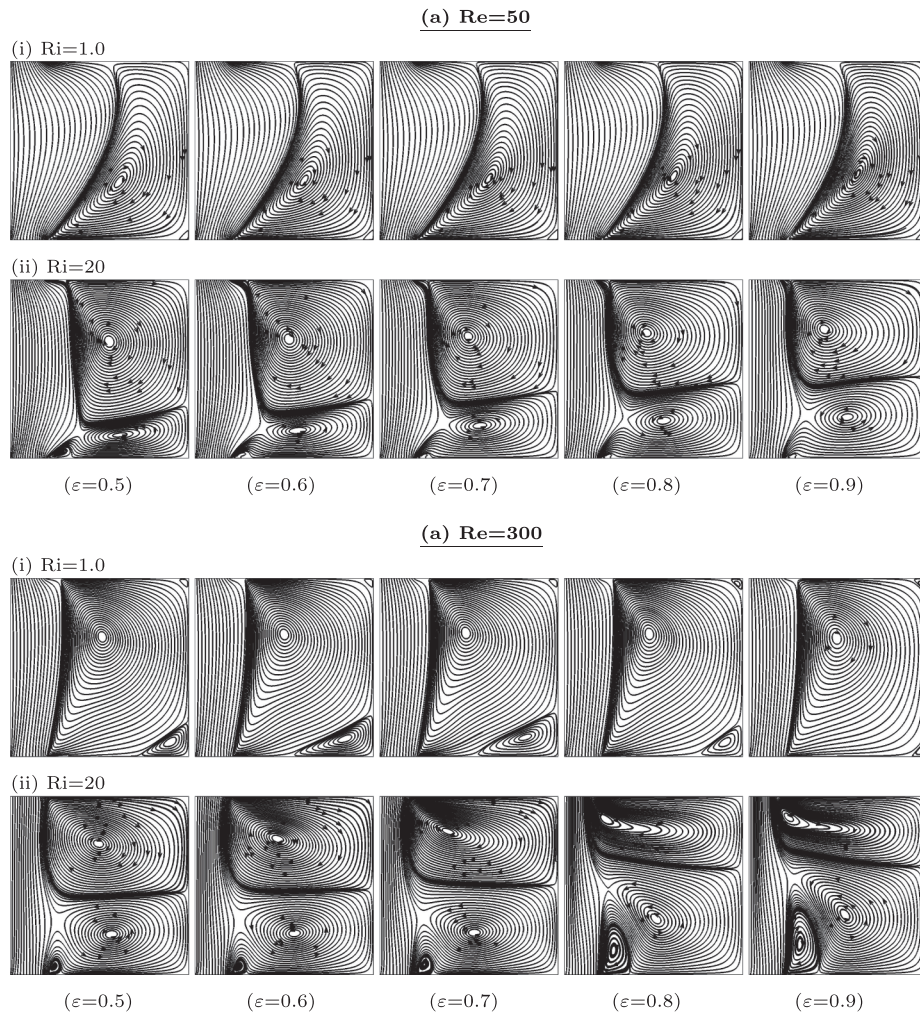


**Fig. 13.** Streamlines patterns for different  $\epsilon$  (0.5–0.9), at (a)  $Re = 50$  and (b)  $Re = 300$ , for (i)  $Ri = 1.0$  and (ii)  $Ri = 20$ , at  $d/H = 0.2$ ,  $Da = 1.0$  and  $K_r = 100$ .

conductivity ratio.

To estimate the influence of porosity  $\epsilon$  during the porous enclosure, the porosity values vary from 0.5 to 0.95 with an increment of 0.1, maintaining Darcy number (permeability) at a constant level of  $Da = 1.0$ . Figs. 13 and 14 display the flow and thermal behaviours, respectively, in the enclosure as the porosity increases, at  $Re = 50$  and 300, and at  $Ri = 1.0$  and 20, and at constant  $d/H=0.2$  and  $K_r=100$ . Commonly known, the actual flow speed stimulated by the inflow and/or the buoyancy forces impacts the performance of convection heat transfer. Thus, when the flow speed is low, the pure natural convection mode of heat transfer is the dominant; while, when the flow speed increases gradually with increasing Reynolds number and Richardson number, the mixed convection mode is generally developed, and then turns into the forced convection. It is found that at low  $Ri = 1.0$ , the entire flow field exhibits a single clockwise-rotating vortex representing the forced convection, and the vortex intensity increases with increasing Reynolds number from 50 to 300. At the same Reynolds number, the vortex intensity also increases as the porosity increases because larger porosity means larger flow volume passing. For more heating at higher  $Ri = 20$ , the action of aiding buoyancy force becomes larger than that

from the shear force, and it controls the flow field at low Reynolds number, producing twin vortices with conflicting rotational directions. It is seen that more stronger double eddies are induced as the porosity increases. Indeed, the reason behind that is a greater porosity promotes a more powerful influence of aiding buoyancy force at the same Richardson number, with additional effect as Reynolds number increases to 300, generating multi-vortices in the flow field. The isotherms lines show that the thermal region in general shrinks with increasing the porosity due to the increase in the convective flow volume. This effect is very obvious at  $Ri = 20$ , as higher Richardson number with higher porosity induce greater buoyancy forces assisting the forced flow, but is less important at smaller  $Re = 50$ . However, the porosity effect becomes more significant at higher  $Re = 300$ , which corresponds to the contribution of the main forced flow together with the assisted buoyancy forces. By comparing the isotherms lines shown in Fig. 14, it appears that the fluid thermal boundary layer on the hot wall decreases as the porosity increases, proposing high temperature gradients that contributes in removing more energy by convection.

Figs. 15 and 16 present the variations of the convective heat transfer  $N_m$  with the porosity at two values of thermal conductivity ratios of  $K_r =$

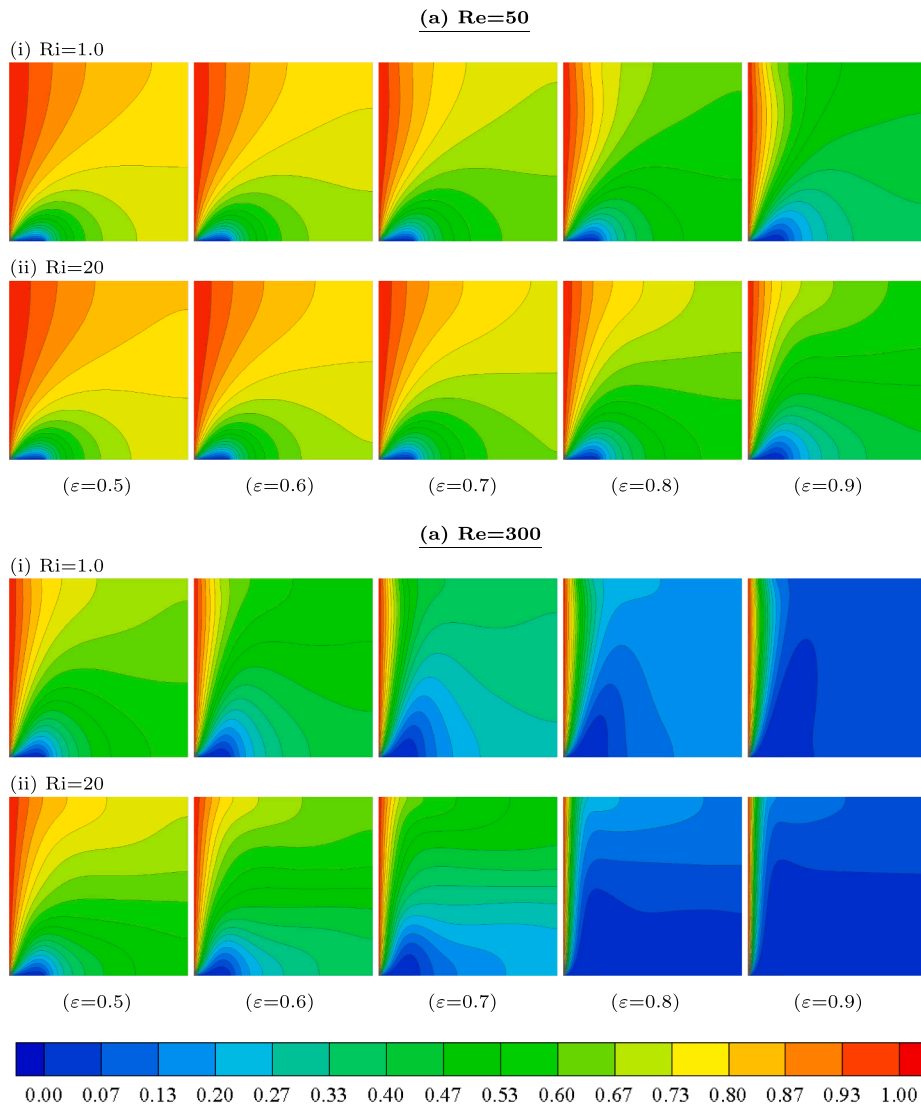


**Fig. 14.** Isotherms patterns for different  $\epsilon$  (0.5–0.9), at (a)  $Re = 50$  and (b)  $Re = 300$ , for (i)  $Ri = 1.0$  and (ii)  $Ri = 20$ , at  $d/H = 0.2$ ,  $Da = 1.0$  and  $K_r = 100$ .

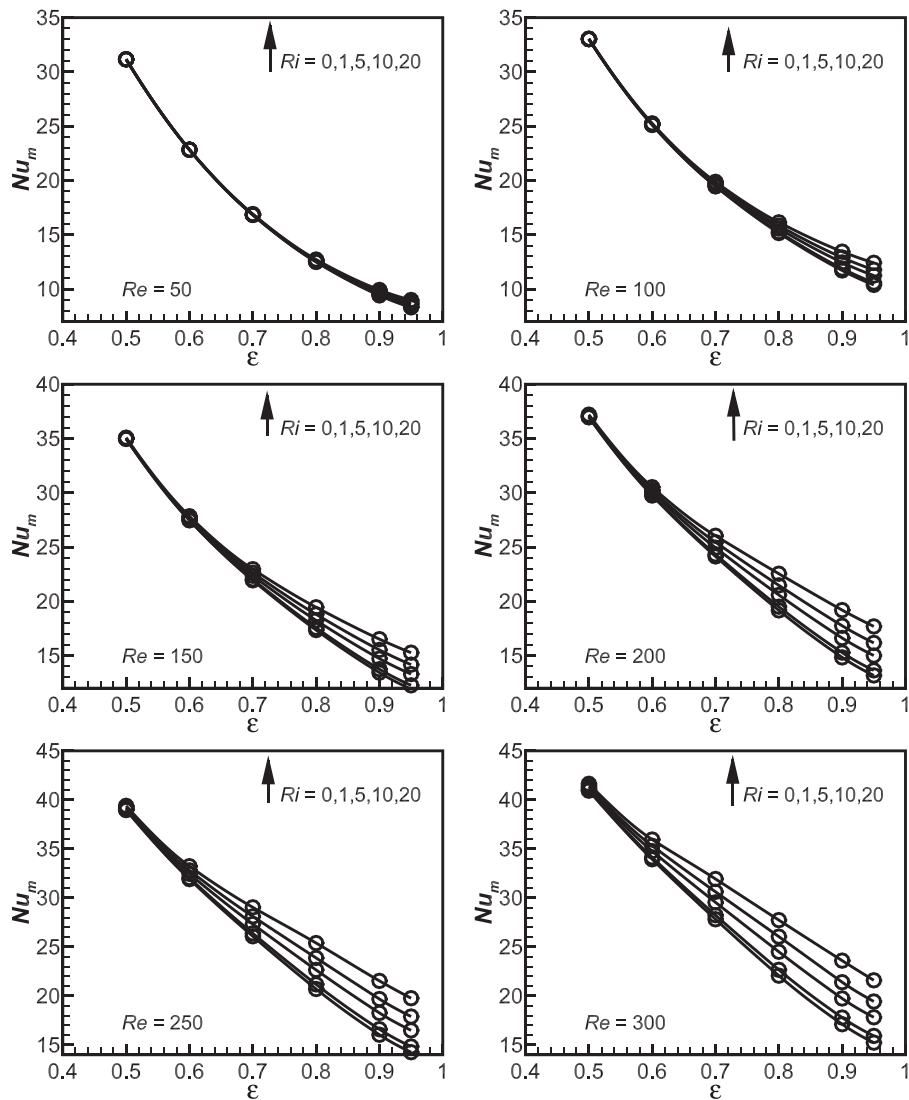


Fig. 15. Mean Nusselt number  $Nu_m$  with  $\varepsilon$  for different  $Re$  and  $Ri$ , at  $d/H = 0.2$ ,  $Da = 1.0$  and  $K_r = 100$ .

100 and  $10^5$ , respectively, and for different Reynolds and Richardson numbers. Interestingly, the figures show that the increase in the porosity leads to a significant decrease in  $Nu_m$ . In fact, the existence of the porous material hinders the main driven-flow with a high resistance in the proximity of the heat source. However, by raising the porosity of the porous medium, the permeability increases, increasing the fluid motion and generating a further high-velocity sweeping flow. Thereby, more convective heat should be removed at the same Reynolds and Richardson numbers. Indeed, the reason for the reduction in  $Nu_m$  as the porosity increases, shown in Figs. 15 and 16, is due to the big contribution of the porosity in decreasing the effective thermal conductivity in Eq. (10), and then decreasing  $Nu_m$  in Eq. (15). Therefore, the reduction effect becomes more pronounced at higher conductivity ratio as shown in Fig. 16.

## 5. Conclusions

A numerical analysis is conducted in this study to investigate two-dimensional, unsteady mixed convective fluid flow and heat transfer

in an air-saturated porous square enclosure. The enclosure is vertically-ventilated; thus the air enters from the bottom wall throughout an inlet slot and exits from the top wall via an outlet port, with a vertical left wall being isothermally-heated, and the remaining walls being insulated. The Brinkman-Forchheimer-extended Darcy model coupled with the one-equation energy model, are used for describing the flow and thermal characteristics. The chosen governing parameters are varied as follows: Richardson number ( $0 \leq Ri \leq 30$ ), Reynolds number ( $50 \leq Re \leq 300$ ), Darcy number ( $0.01 \leq Da \leq 100$ ), the solid/fluid thermal conductivity ratio ( $1 \leq K_r \leq 10^5$ ), the porosity ( $0.5 \leq \varepsilon \leq 0.95$ ), and the inlet/outlet openings width ( $0 \leq d/H \leq 0.3$ ). The obtained results draw the following conclusions:

1. The existence of a porous material inside a vented enclosure augments generally the convection heat transfer, and increases the thermal performance.
2. The mean Nusselt number ( $Nu_m$ ) increases significantly with an increase in Reynolds number and/or Richardson number.

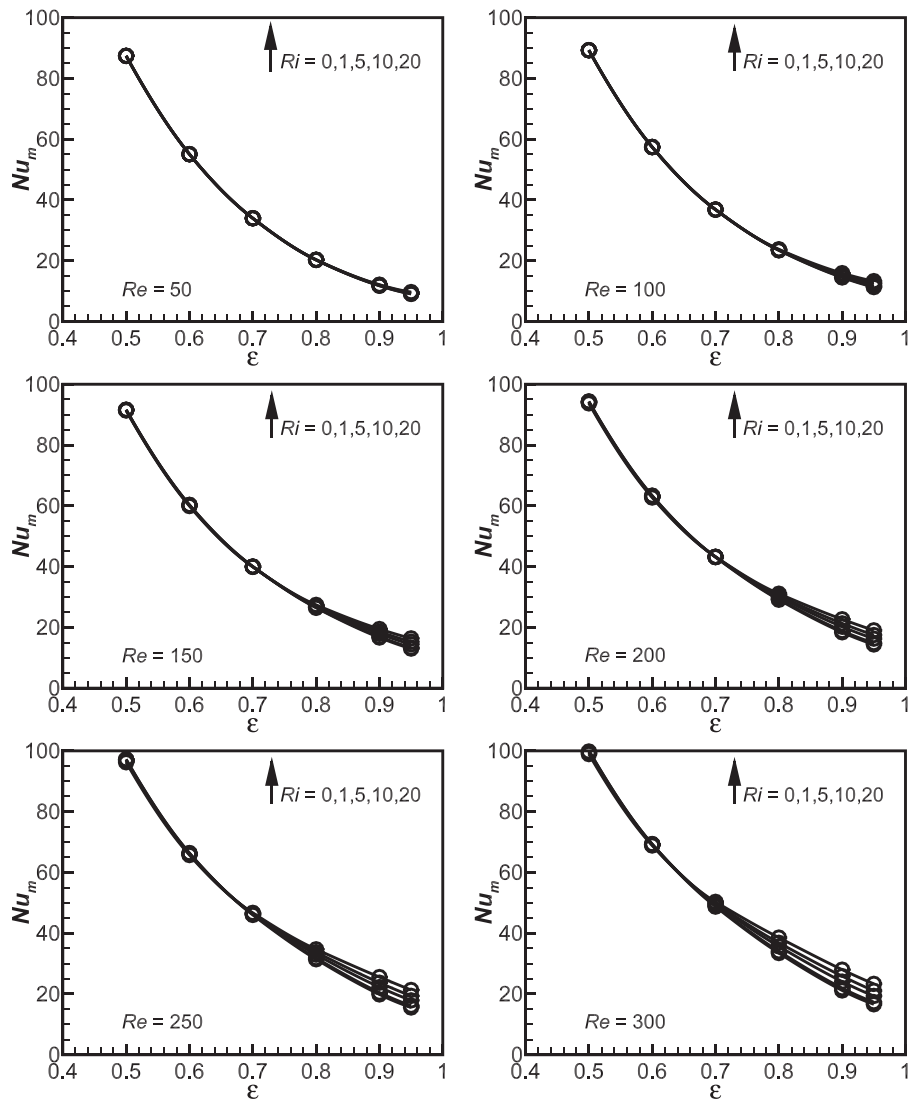


Fig. 16. Mean Nusselt number  $Nu_m$  with  $\varepsilon$  for different  $Re$  and  $Ri$ , at  $d/H = 0.2$ ,  $Da = 1.0$  and  $K_r = 10^5$ .

- $Nu_m$  increases as the inlet/outlet openings width increases over the entire ranges of Reynolds and Richardson numbers. Also, an optimum value of  $d/H = 0.25$  is found for obtaining maximum  $Nu_m$ .
- $Nu_m$  increases as Darcy number increases, with more considerably effect at higher Reynolds and Richardson numbers.
- $Nu_m$  increases appreciably with raising the thermal conductivity ratio, for all inflow (Reynolds number) and heating (Richardson number) conditions. Also, changing the conductivity ratio does not have an observable effect on the flow behaviour; however, the noticeable impact of this parameter is observed to be on the thermal behaviour.
- Importantly, although the fluid thermal boundary layer on the heated vertical surface is shown to decrease as the porosity increases, e.g. proposing high temperature gradients that can contribute in removing more energy by convection, increasing the porosity is found to decrease remarkably  $Nu_m$ .

#### Funding

This research did not receive any specific grant from funding agencies in the public, commercial, or not-for-profit sectors.

#### CRediT authorship contribution statement

**Wissam H. Alawee:** Writing - original draft, Resources. **Gazy F. Al-Sumaily:** Conceptualization, Data curation, Formal analysis, Writing - review & editing. **Hayder A. Dhahad:** Methodology, Validation, Investigation, Visualization. **Mark C. Thompson:** Software, Supervision, Project administration.

#### Declaration of Competing Interest

The authors declare that they have no known competing financial interests or personal relationships that could have appeared to influence the work reported in this paper.

#### Acknowledgement

This research was supported in part by the Monash eResearch Centre and eSolutions-Research Support Services through the use of the Mon-ARCH HPC Cluster.

## References

- [1] M. Izadi, M.M. Shahmardan, M. Norouzi, A.M. Rashidi, A. Behzadmehr, Cooling performance of a nanofluid flow in a heat sink microchannel with axial conduction effect, *Applied Physics A* 117 (2014) 1821–1833.
- [2] M. Izadi, P. Hashemi, A. Yasuri, A. Chamkha, Mixed convection of a nanofluid in a three-dimensional channel, *Journal of Thermal Analysis and Calorimetry* 136 (2019) 2461–2475.
- [3] M. Izadi, H.F. Öztop, M.A. Sheremet, S.A. Mehryand, N. Abu-Hamdeh, Coupled FHD–MHD free convection of a hybrid nanoliquid in an inverted T-shaped enclosure occupied by partitioned porous media, *Numerical Heat Transfer, Part A: Applications* 76 (2019) 479–498.
- [4] M. Izadi, S.A. Mohammadi, S.A.M. Mehryan, T. Yang, M.A. Sheremet, Thermogravitational convection of magnetic micropolar nanofluid with coupling between energy and angular momentum equations, *International Journal of Heat and Mass Transfer* 149 (2019), 118748.
- [5] M. Izadi, R. Mohebbi, H. Sajjadi, A.A. Delouei, LTNE modelling of Magneto-Ferro natural convection inside a porous enclosure exposed to nonuniform magnetic field, *Physica A* 535 (2019), 122394.
- [6] R. Mohebbi, S.A. Mehryan, M. Izadi, O. Mahian, Natural convection of hybrid nanofluids inside a partitioned porous cavity for application in solar power plants, *Journal of Thermal Analysis and Calorimetry* 137 (2019) 1719–1733.
- [7] M. Izadi, Effects of porous material on transient natural convection heat transfer of nano-fluids inside a triangular chamber, *Chinese Journal of Chemical Engineering* 28 (2020) 1203–1213.
- [8] M. Izadi, B. Bastani, M.A. Sheremet, Numerical simulation of thermogravitational energy transport of a hybrid nanoliquid within a porous triangular chamber using the two-phase mixture approach, *Advanced Powder Technology* 31 (2020) 2493–2504.
- [9] M. Izadi, M. Javanahram, S.M.H. Zadeh, D. Jing, Hydrodynamic and heat transfer properties of magnetic fluid in porous medium considering nanoparticle shapes and magnetic field-dependent viscosity, *Chinese Journal of Chemical Engineering* 28 (2020) 329–339.
- [10] M. Izadi, M. Ghalambaz, S.A.M. Mehryan, Location impact of a pair of magnetic sources on melting of a magneto-Ferro phase change substance, *Chinese Journal of Physics* 65 (2020) 377–388.
- [11] M. Izadi, M.A. Sheremet, S.A.M. Mehryan, Natural convection of a hybrid nanofluid affected by an inclined periodic magnetic field within a porous medium, *Chinese Journal of Physics* 65 (2020) 447–458.
- [12] M. Izadi, M.A. Sheremet, S.A.M. Mehryan, I. Pop, H.F. Öztop, N. Abu-Hamdeh, MHD thermogravitational convection and thermal radiation of a micropolar nanoliquid in a porous chamber, *International Communications in Heat and Mass Transfer* 110 (2020), 104409.
- [13] S.M. Seyyedi, A.S. Dogonchi, M. Hashemi-Tilehnoe, M. Waqas, D.D. Ganji, Entropy generation and economic analyses in a nanofluid filled L-shaped enclosure subjected to an oriented magnetic field, *Applied Thermal Engineering* 168 (2020), 114789.
- [14] S.M. Seyyedi, A.S. Dogonchi, M. Hashemi-Tilehnoe, M. Waqas, D.D. Ganji, Investigation of entropy generation in a square inclined cavity using control volume finite element method with aided quadratic Lagrange interpolation functions, *International Communications in Heat and Mass Transfer* 110 (2020), 104398.
- [15] K.M. Khanafer, A.J. Chamkha, Mixed convection flow in a lid-driven enclosure filled with a fluid-saturated porous medium, *International Journal of Heat and Mass Transfer* 42 (1999) 2465–2481.
- [16] A.M. Al-Amiri, Analysis of momentum and energy transfer in a lid-driven cavity filled with a porous medium, *International Journal of Heat and Mass Transfer* 43 (2000) 3513–3527.
- [17] K.M. Khanafer, K. Vafai, Double-diffusive mixed convection in a lid-driven enclosure filled with a fluid-saturated porous medium, *Numerical Heat Transfer, Part A, Applications* 42 (2002) 465–486.
- [18] H.F. Öztop, Combined convection heat transfer in a porous lid-driven enclosure due to heater with finite length, *International Communications in Heat and Mass Transfer* 33 (2006) 772–779.
- [19] T.M. Jeng, S.C. Tzeng, Heat transfer in a lid-driven enclosure filled with water-saturated aluminium foams, *Numerical Heat Transfer, Part A, Applications* 54 (2008) 178–196.
- [20] E. Vishnuvardhanarao, M.K. Das, Laminar mixed convection in a parallel two-sided lid-driven differentially heated square cavity filled with a fluid-saturated porous medium, *Numerical Heat Transfer, Part A, Applications* 53 (2008) 88–110.
- [21] T. Basak, S. Roy, S.K. Singh, I. Pop, Analysis of mixed convection in a lid-driven porous square cavity with linearly heated side wall(s), *International Journal of Heat and Mass Transfer* 53 (2010) 1819–1840.
- [22] S.E. Ahmed, Mixed convection in thermally anisotropic non-Darcy porous medium in double lid-driven cavity using Bejan's heatlines, *Alexandria Engineering Journal* 55 (2016) 299–309.
- [23] Y. Wang, G. Qin, Accurate numerical simulation for non-Darcy double-diffusive mixed convection in a double lid-driven porous cavity using SEM, *Numerical Heat Transfer, Part A, Applications* 75 (2019) 598–615.
- [24] L. Wang, W. Wang, Y. Cai, D. Liu, F. Zhao, Effects of porous fins on mixed convection and heat transfer mechanics in lid-driven cavities: full numerical modelling and parametric simulations, *Transport in Porous Media* 132 (2020) 495–534.
- [25] S. Mahmud, I. Pop, Mixed convection in a square vented enclosure filled with a porous medium, *International Journal of Heat and Mass Transfer* 49 (2006) 2190–2206.
- [26] K. Murthy, R. Kumar, Non-Darcy mixed convection in a porous square enclosure under suction/injection effects with a non-isothermal vertical wall, *Numerical Heat Transfer, Part A, Applications* 57 (2010) 580–602.
- [27] R. Kumar, K. Murthy, Mixed convection in a non-Darcian fluid saturated square porous enclosure under multiple suction effect, *International Journal of Heat and Mass Transfer* 53 (2010) 5764–5773.
- [28] K. Murthy, R. Kumar, Darcy mixed convection in a fluid saturated square porous enclosure under multiple suction effect, *International Journal of Numerical Methods for Heat and Fluid Flow* 21 (2011) 602–617.
- [29] T. Behzadi, K.M. Shirvan, S. Mirzakanlari, A.A. Sheikhrabat, Numerical Simulation on Effect of Porous Medium on Mixed Convection Heat Transfer in a Ventilated Square Cavity, in: *International Conference on Computational Heat and Mass Transfer*, vol. 127, *Procedia Engineering*, 2015, pp. 221–228.
- [30] H.A. Dhahad, G.F. Al-Sumaily, W.H. Alawee, M.C. Thompson, Aiding and opposing re-circulating mixed convection flows in a square vented enclosure, *Thermal Science and Engineering Progress* 19 (2020) (article no. 100577).
- [31] M. Kaviany, *Principles of Heat Transfer in Porous Media*, Springer-Verlag, 1995.
- [32] D.A. Nield, A. Bejan, *Convection in Porous Media*, third ed., Springer Science+Business Media, New York, NY, USA, 2006.
- [33] S.V. Patankar, *Numerical Heat Transfer and Fluid Flow*, Hemisphere Publishing Corporation, New York, 1980.
- [34] J.H. Ferziger, M. Peric, *Computational Methods for Fluid Dynamics*, Springer, Berlin, 1997.
- [35] M. Kumari, S. Jayanthi, Non-darcy non-newtonian free convection flow over a horizontal cylinder in a saturated porous medium, *International Communications of Heat and Mass Transfer* 31 (2004) 1219–1226.
- [36] I. Pop, M. Kumari, G. Nath, Free convection about cylinders of elliptic cross section embedded in a porous medium, *International Journal of Engineering Sciences* 30 (1992) 35–45.
- [37] K. Yih, Coupled heat and mass transfer by natural convection adjacent to a permeable horizontal cylinder in a saturated porous medium, *International Communications of Heat and Mass Transfer* 26 (1999) 431–440.